Available online at www.sciencedirect.com
ScienceDirect
Journal of Power Sources 160 (2006) 1163–1169
JOURNAL OF POWER SOURCES
www.elsevier.com/locate/jpowsour

Optimization of a water–gas shift reactor over a Pt/ceria/alumina monolith

A.S. Quiney, G. Germani, Y. Schuurman *

Institut de Recherches sur la Catalyse-CNRS, 2 Avenue A. Einstein, 69626 Villeurbanne, France

Received 27 January 2006; received in revised form 3 March 2006; accepted 9 March 2006
Available online 27 April 2006

Abstract

The water–gas shift (WGS) reaction is an important step in the purification of hydrogen for fuel cells. It lowers the carbon monoxide content and produces extra hydrogen. The constraints of automotive applications render the commercial WGS catalysts unsuitable. Pt/ceria catalysts are cited as promising catalysts for onboard applications as they are highly active and non-pyrophoric. This paper reports on a power law rate expression for a $Pt/CeO_2/Al_2O_3$ catalyst. This rate equation is used to compare different reactor configurations for an onboard water–gas shift reactor. A one-dimensional heterogeneous model that accounts for the interfacial and intraparticle gradients has been used to optimize a dual stage adiabatic monolith reactor.

Keywords: Hydrogen purification; CO clean-up; Optimal temperature; Fuel cells

1. Introduction

Hydrogen is a fuel well adapted for the onboard generation of electricity by means of fuel cells. Several fossil fuels can be reformed to generate hydrogen for automotive applications. The use of gasoline or diesel oil is attractive for onboard generation of hydrogen, especially for Auxiliary Power Unit (APU) systems coupled to Internal Combustion Engines (ICE), as both APU and ICE systems would then make use of the same fuel. Generation of hydrogen is performed by a fuel processor which consists of several different units, mainly to reduce the carbon monoxide content of the reformate mixture since the proton-exchange membrane (PEM) fuel cells have a very low tolerance towards CO, namely less than 50 ppm [1]. One of these units is the water–gas shift reactor (WGS). This reaction converts CO into CO_2 by the reaction with water over a suitable catalyst and provides additional hydrogen. The reaction generally attains thermodynamic equilibrium. The most active industrial catalysts are iron-chromium catalyst for the high temperature shift and copper-based materials operated in the temperature range between 180 and 250 °C. The volume of the LT-WGS takes a considerable part of the overall fuel processor due to the low operating temperatures. Besides high activity, others requirements have to be fulfilled for automotive applications: fast response, long lifetime and non-pyrophoric materials. Moreover, the catalyst needs to be attrition resistant and therefore monolith-supported catalysts are preferable. However, on the basis of the intrinsic rate the use of monoliths leads to heavier and more voluminous systems compared to fixed bed reactors. This might change if internal diffusion limitations dominate the global reaction rate. Trambouze and Euzen [2] have derived a criteria for first-order irreversible reaction to compare spherical particles with monoliths as a function of the characteristic catalyst size and Thiele modulus and show that monoliths can outperform solid catalysts on a volume basis for a Thiele modulus greater than 10.

The current study focuses on the simulation and optimization of a monolith reactor for the CO conversion for onboard applications. A kinetic expression developed for an in-house developed $Pt/CeO_2/Al_2O_3$ catalyst has been used. These catalysts are cited as promising catalysts for onboard applications [3–7] as they are highly active and non-pyrophoric.

2. Reactor model

A one-dimensional heterogeneous model that accounts for the interfacial and intraparticle gradients has been used [8]. The one-dimensional heterogeneous model is used to simulate a single monolith channel as well as the fixed bed configuration. For

* Corresponding author. Tel.: +33 47244548; fax: +33 472445399.
E-mail address: schuurman@catalyse.cnrs.fr (Y. Schuurman).

0378-7753/$ – see front matter © 2006 Elsevier B.V. All rights reserved.
doi:10.1016/j.jpowsour.2006.03.019

Nomenclature

a_v	external surface area per unit reactor ($m_s^2\ m_r^{-3}$)
C_j	molar concentration of species j ($mol\ m_f^{-3}$)
C_P	heat capacity of the fluid phase ($J\ mol^{-1}\ K^{-1}$)
d_h	hydraulic diameter (m)
d_p	catalyst particle size (m)
$\mathcal{D}$	molecular diffusion coefficient ($m^2\ s^{-1}$)
D_{Aris}	dispersion coefficient ($m^2\ s^{-1}$)
D_{eCO}	effective diffusion coefficient of CO ($m_f^3\ m_s^{-1}\ s^{-1}$)
Da	Damköhler number, $Da = r_{CO}\delta_{wash}d_h/4\varepsilon_b C_{CO}\mathcal{D}$
E_{act}	activation energy ($J\ mol^{-1}$)
F_j	molar flow rate of species j ($mol\ s^{-1}$)
F_t	total molar flow ($mol\ s^{-1}$)
h_f	heat transfer coefficient for film ($J\ m_s^{-2}\ s^{-1}\ K^{-1}$)
k_j	mass transfer coefficient from gas to solid interface for species j ($m_f^3\ m_s^{-2}\ s^{-1}$)
K_{eq}	overall equilibrium constant
l	distance inside the monolith channel (m)
L	reactor length (m)
Nu	Nusselt number, $Nu = h_f d_h/\lambda_e$
P_j	partial pressure of component j (bar)
Pr	Prandtl number, $Pr = C_P\mu/\lambda_e$
r_{CO}	rate of CO disappearance ($mol\ kg_{cat}^{-1}\ s^{-1}$)
R	gas constant ($J\ mol^{-1}\ K^{-1}$)
Re	Reynolds number, $Re = \rho u d_h/\mu$
Re_p	Reynolds number based on catalyst particle size, $Re_p = \rho u d_p/\mu$
Sc	Schmidt number, $Sc = \mu/\rho D$
Sh	Sherwood number, $Sh = k_j d_h/D$
T	temperature (K)
u	gas velocity ($m\ s^{-1}$)
V	reactor volume (m_r^3)
W	catalyst mass (kg)
X_{CO}	CO conversion
y'_j	mole fraction of component j at the reactor inlet with respect to the mole fraction of CO
z	distance inside the catalyst (ms)

Greek letters

β	reversibility factor
δ_{wash}	thickness of the washcoat (m_s)
ΔH_R	enthalpy of reaction ($J\ mol^{-1}$)
ΔS_R	entropy of reaction ($J\ mol^{-1}\ K^{-1}$)
λ_e	effective thermal conductivity of the solid phase ($J\ m^{-1}\ s^{-1}\ K^{-1}$)
μ	viscosity of the gas mixture (Pa s)
ρ	density of the gas mixture ($kg\ m_f^{-3}$)
ρ_s	catalyst density ($kg\ m_s^{-3}$)

Superscripts

0	inlet
p	inside solid phase washcoat or particle
s	surface

Subscripts

j	component or species
f	fluid phase
r	reactor
s	solid phase
t	total

the two cases different correlations for heat- and mass transfer coefficients are used. The mass- and heat balances on the level of the catalyst depend on its geometry. No light-off or ignition is expected due to the reversible and mildly exothermic nature of the reaction. This leads to a smooth variation of the *Nu* and *Sh* numbers as a function of the axial coordinate [9] making a one-dimensional model for the monolith channel adequate. The coefficients for mass and heat transfer in the monolith reactor are those calculated from the relations proposed by Groppi et al. [10]. For the packed bed reactor the relations of Wakao and Kaguei [11] have been used. The correlations for heat transfer are given in Table 1. Replacing the *Nu* numbers by the *Sh* numbers and the *Pr* numbers by the *Sc* numbers gives the mass transfer correlations.

Axial dispersion in a monolith channel operated in the laminar flow regime can be neglected when [12]:

$$\frac{uL}{D_{Aris}} > 100 \tag{1}$$

where D_{Aris} is the dispersion coefficient given by the Aris equation [13]:

$$D_{Aris} = \frac{u^2 d_h^2}{192\mathcal{D}} + \mathcal{D} \tag{2}$$

For all conditions used in this study ($u > 0.2\ m\ s^{-1}$, $L > 0.4$ m, $D_{Aris} \approx 4 \times 10^{-5}\ m^2\ s^{-1}$) the left-hand term of Eq. (1) is always greater than 2000; thus, the axial dispersion can be neglected. Cordierite monoliths are poor heat conductors and are only operated adiabatically. Therefore, this study is restricted to adiabatic reactors only. The heat capacities were taken from the property data bank by Reid et al. [14]. The density of the mixture has been calculated by the ideal gas law. Due to the small flow resistance of monoliths the pressure drop over the reactor is negligible

Table 1
Correlations for heat transfer

Square channel monolith

$$2Nu = Nu_H - Da\frac{Nu_H}{Nu_T} + \sqrt{\left(Nu_H - Da\frac{Nu_H}{Nu_T}\right)^2 + 4DaNu_H} \tag{11}$$

$$Nu_H = 3.095 + 8.933\left(\frac{1000}{l^*}\right)^{-0.5386}\exp\left(-\frac{6.7275}{l^*}\right) \tag{12}$$

$$Nu_T = 2.977 + 6.854\left(\frac{1000}{l^*}\right)^{-0.5174}\exp\left(-\frac{42.49}{l^*}\right) \tag{13}$$

$$l^* = RePr\frac{d_h}{l} \tag{14}$$

Packed bed reactor

$$Nu = 2 + 1.1Re_p^{0.6}Pr^{0.33} \tag{15}$$

Table 2
Model equations

Fluid phase

$$\frac{dF_j}{dV} = a_v k_j (C^s_{CO} - C_{CO}) \quad \text{mol s}^{-1}\,\text{m}^{-3} \tag{3}$$

$$\frac{dT}{dV} = \frac{a_v h_f (T^s - T)}{C_P F_t} \quad \text{K m}^{-3} \tag{4}$$

Solid phase (slab geometry)

$$D_{ej}\left[\frac{\partial^2 C^p_{CO}}{\partial z^2}\right] = \rho_s r_{CO} \quad \text{mol s}^{-1}\,\text{m}^{-3}_{cat} \tag{5}$$

$$\lambda_e\left[\frac{\partial^2 T^p}{\partial z^2}\right] = \rho_s(-\Delta H_R) r_{CO} \quad \text{J s}^{-1}\,\text{m}^{-3}_{cat} \tag{6}$$

Initial conditions

$$V = 0: \quad C_j = C^0_j \wedge T = T^0 \tag{7}$$

Boundary conditions

$$z = 0: \quad \frac{\partial C^p_{CO}}{\partial z} = \frac{\partial T^p}{\partial z} = 0 \tag{8}$$

$$z = \delta_{wash}: \quad k_{CO}(C^s_{CO} - C_{CO}) = -D_{eCO}\frac{\partial C^p_{CO}}{\partial z} \quad \text{mol s}^{-1}\,\text{m}^{-2}_{cat} \tag{9}$$

$$z = \delta_{wash}: \quad h_f(T^s - T) = -\lambda_e \frac{\partial T^p}{\partial z} \quad \text{J s}^{-1}\,\text{m}^{-2}_{cat} \tag{10}$$

and therefore the momentum equation has not been taken into account. Transport inside the catalyst layer is assumed to be by Fickian diffusion only, using an effective intraparticle diffusion coefficient. The binary molecular diffusion coefficients are calculated from the Füller–Schettler–Giddings relation [14] and then the Wilke equation is used to calculate the diffusivities of the mixture [14]. Adapting the above hypotheses leads to the mathematical equations reported in Table 2.

Since the reaction is stoichiometrically single, continuity equations for only CO are sufficient to calculate the concentration profiles.

2.1. Solution procedure

The set of equations to be solved consists of two ordinary non-linear first-order differential equations that form a set of initial value problem coupled to two non-linear second-order differential equations that make up a set of boundary value problem. The first-order differential equations were numerically integrated using the ODEPACK library [15]. At each node of the computational grid for the fluid field equations the concentration and temperature gradients for a single particle are calculated including the surrounding film. This is accomplished by solving the second-order equations using the method of lines and the ODEPACK solver [16]. A number of physical properties and other variables (e.g. ρ, C_P, u and ΔH) depend on the temperature, pressure or flow composition. These are updated after each integration step in a separate subroutine. This subroutine also evaluates the correlations for the mass and heat transfer coefficients and the thermal conductivity. All this is implemented in a FORTRAN code.

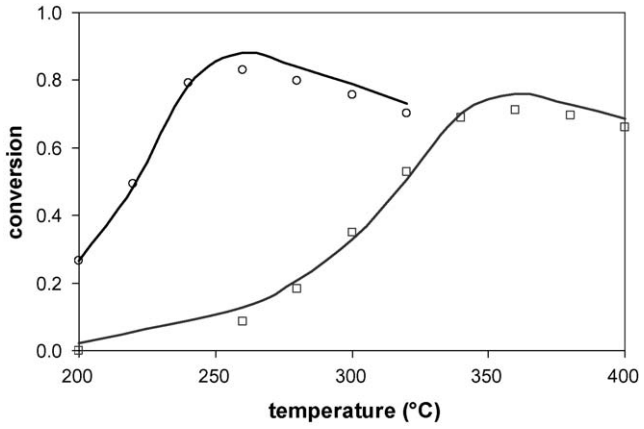

Fig. 1. Experimental (symbols) and calculated (lines) conversion as a function of temperature for two sets of conditions: (◯) $W/F = 4.84$ kg s mol^{-1}, Ar 23.1%, H_2 33.8%, CO_2 13.0%, CO 2.6%, H_2O 27.5%; (□) $W/F = 1.21$ kg s mol^{-1}, Ar 26.2%, H_2 32.2%, CO_2 8.4%, CO 9.6%, H_2O 23.0%.

3. Kinetic model

The rate equation used for the simulations has been obtained by a regression analysis of a large data set (approximately 70 experiments) using integral conditions under the absence of mass and heat transfer limitations over the $Pt/CeO_2/Al_2O_3$ catalyst [17].

$$r_{CO} = 4.3 \times 10^5 \exp\left(\frac{-76.8 \times 10^3}{RT}\right) \times P^{0.13}_{CO} P^{0.49}_{H_2O} P^{-0.45}_{H_2} P^{-0.12}_{CO_2}(1-\beta) \quad \text{mol s}^{-1}\,\text{kg}^{-1}_{cat} \tag{16}$$

$$\beta = \frac{P_{H_2} P_{CO_2}}{K_{eq} P_{CO} P_{H_2O}} \tag{17}$$

From [18]

$$K_{eq} = \exp\left(\frac{-36.0}{R}\right) \exp\left(\frac{38,060}{RT}\right) \tag{18}$$

The reaction is strongly inhibited by hydrogen and to a lesser extent by carbon dioxide. The reaction rate hardly depends on the partial pressure of carbon monoxide, but it increases with increasing partial pressures of water as long as the thermodynamic equilibrium is not attained.

A typical fit of the data as a function of temperature is shown in Fig. 1.

4. Operating conditions

4.1. Gas composition

The composition of the gas mixture entering the WGS unit is typical of an autothermal reformer, presented in Table 3. The oxygen necessary to supply the heat to drive the steam reforming comes from air thus introducing a significant amount of nitrogen. The production of 5 kW of electric power requires a hydrogen flow of 43 mmol s^{-1}, assuming a hydrogen efficiency of 80% for the fuel cell.

Table 3
Gas composition for the WGS unit

Components	Volume percent	Molar flow (mmol s^{-1})
CO	10.0	13.5
H_2O	23.0	31.0
H_2	32.0	43.2
CO_2	8.0	10.8
N_2	27.0	36.5

Table 4
Monolith reactor used for the simulations

Number of channels per square inch (cpsi)	400
Inner channel diameter before coating (mm)	1.1
Wall thickness (mm)	0.15
Washcoat porosity	0.4
Washcoat tortuosity	4.0
BET washcoat ($m^2\,g^{-1}$)	69
Washcoat cross-sectional area (mm^2)	0.166
Washcoat density ($kg\,m^{-3}$)	1500

4.2. Pressure

The pressure for a fuel processor is usually comprised between 3 and 5 bar mainly to facilitate the water management. Therefore, the pressure of the WGS unit has been fixed to 3 bar.

4.3. Reactor dimensions

A 400 cells per square inch (cpsi) monolith with an outer diameter of 10 cm has been chosen. This implies 4867 equal monolith channels over which the total flow is distributed. Once the catalyst amount has been calculated the length of the monolith can be calculated from the washcoat cross-section and the washcoat density both given in Table 4.

4.4. Constraints

A preferential CO oxidation unit follows the WGS unit in order to lower the CO level below 50 ppm. Due to the strong exothermicity of the CO oxidation reaction, the CO inlet concentration should not be too high else the selectivity goals might not be met due to the too high operating temperatures. The maximum outlet CO concentration for the WGS unit is therefore fixed at 1% (10,000 ppm). This implies CO conversion levels of at least 90%.

The formation of small amounts of methane and coke deposits on the catalyst has been observed at reaction temperatures above 400 °C. Therefore, the temperature in this study is limited to 375 °C.

5. Multibed adiabatic reactor

The design of multibed adiabatic reactors with interstage cooling for exothermal reversible reactions is well established [8,19]. All characteristics of this process can be represented on a plot of the conversion versus temperature, as shown in Fig. 2. This plot regroups different curves; the upper curve corresponds

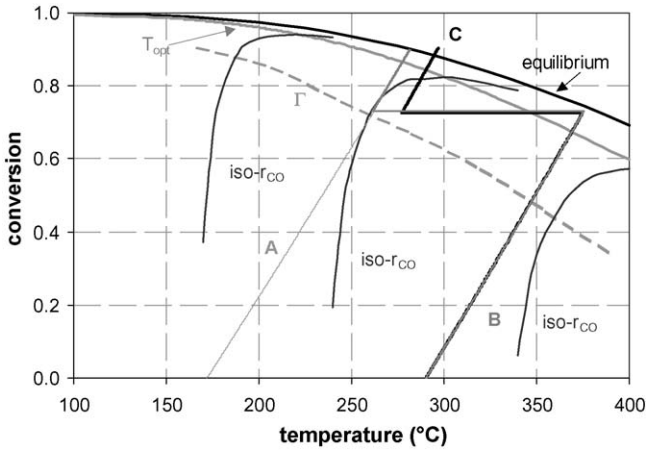

Fig. 2. Characteristics of a reversible exothermic reaction.

to the thermodynamic equilibrium for the CO conversion, the line just below it represents the optimal temperature path. This curve is calculated by taking the derivative of the kinetic equation with respect to the temperature and setting it equal to zero. For any power law rate equation the optimal temperature as a function of the conversion is given by:

$$T_{\text{opt}} = \frac{\Delta H_{\text{R}}}{\Delta S_{\text{R}} - R\,\ln[(1-(\Delta H_{\text{R}}/E_{\text{act}}))\times((y'_{\text{H}_2}-X_{\text{CO}}) \times (y'_{\text{CO}_2}-X_{\text{CO}}))/((1-X_{\text{CO}})(y'_{\text{H}_2\text{O}}-X_{\text{CO}}))]} \tag{19}$$

Notice that the only kinetic parameter in this equation is the activation energy.

The curve below this one is the Γ curve corresponding to the adiabatic optimal path. This curve is calculated by finding the root from:

$$\left(\frac{\delta r_{\text{CO}}}{\delta X_{\text{CO}}}\right)_T + \Delta T_{\text{ad}}\left(\frac{\delta r_{\text{CO}}}{\delta T}\right)_{X_{\text{CO}}} = 0 \tag{20}$$

with

$$\Delta T_{\text{ad}} = \frac{-\Delta H_{\text{R}} y_{\text{CO}}}{C_P} \tag{21}$$

The straight lines correspond to the adiabatic operation with a slope equal to ΔT_{ad}. The three curves labeled "iso-r_{CO}" are the "rate contours" and these are obtained by finding the root of $r(X_{\text{CO}}, T) = \text{constant}$ as a function of the temperature. The maxima of the rate-contours curves coincide with the optimal temperature curve.

To find the optimal cascade of reactors in terms of numbers and inlet temperatures becomes computationally expensive if the number of reactors increases. The problem can than be solved by "dynamic programming" [20,21]. In general terms, the first stages are designed around the Γ curve with the reactor outlet temperatures that are beyond the optimal temperature path. The last stages are then around the optimal temperature curve [19].

The WGS unit considered here is restricted to one or two reactors. The interstage cooling has been simulated by either a heat exchanger or by injection of liquid water (at 25 °C). The different configurations considered are shown in Fig. 3.

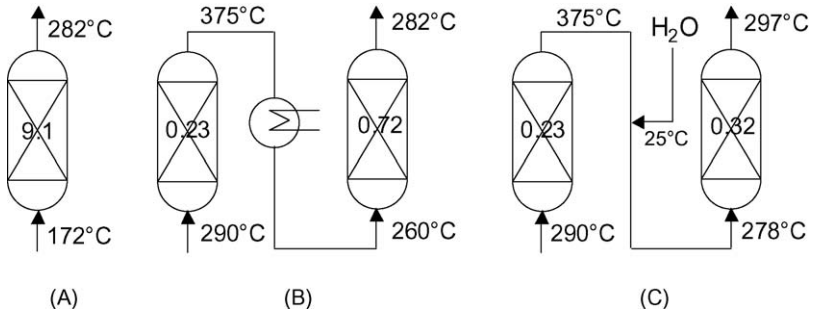

Fig. 3. Different optimized monolith reactor configurations: (A) single stage adiabatic reactor; (B) two-stage adiabatic reactor with heat exchanger; (C) two-stage adiabatic reactor with water injection. The numbers mentioned in the middle of the reactors correspond to the calculated amount of catalyst (kg).

6. Monolith reactor simulation

Fig. 4 shows a scanning electron micrograph of the ceria/alumina washcoat. Due to the nature of the coating process, thicker layers of washcoat are likely to adhere in the corners of the channels. For this sample the layer thickness varies from 15 μm on the side to 100 μm in the corner section. By doing more successive preparations a thicker layer can be achieved; thus, for the simulations a layer thickness of 20 μm on the side to 170 μm in the corner section was used as shown in Fig. 5.

To take into account rigorously (in the absence of axial diffusion) the shape of the washcoat layer in the model a 2D description is necessary. A more simplified procedure consists of calculating the characteristic layer thickness that is equal to the ratio of the cross-sectional area of the washcoat and the wetted perimeter. Whereas the first approach is computationally expensive, the second one does not give the correct result

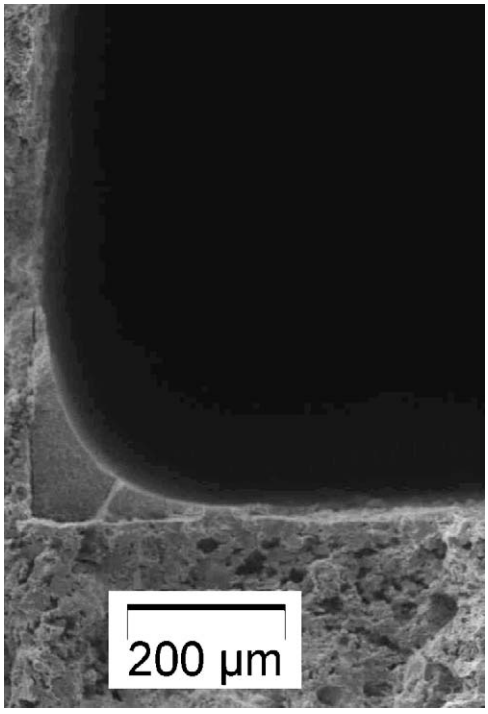

Fig. 4. Scanning electron micrograph of a CeO_2/Al_2O_3 washcoat in a 400 cpsi cordierite monolith.

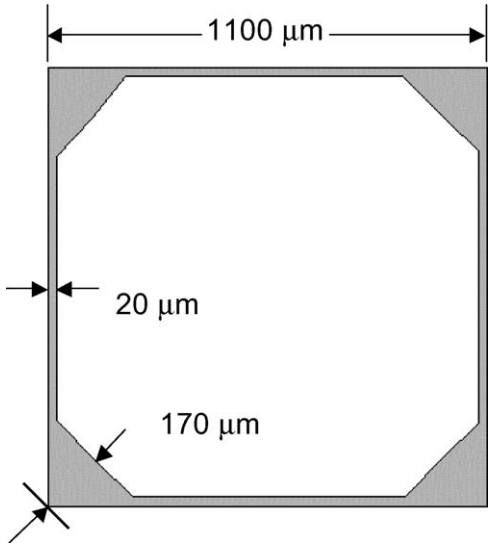

Fig. 5. Schematic drawing of washcoat used in the simulations.

and generally underestimates the diffusion limitations [22]. The approach taken here consists of representing the washcoat by two characteristic lengths, one for the corner sections and one for the sides. Fig. 4 shows a schematic of the washcoat geometry considered. The side sections are slabs with a characteristic length of 20 μm and the characteristic length of 95 μm of the corners is calculated as the cross-sectional area divided by the wetted perimeter. The corner sections represent ∼68% of the washcoat volume and the sides ∼32%. For each section an efficiency factor is calculated and the overall reaction rate amounts to the sum of those corrected for the volume percentages. A characteristic length of 43 μm is calculated if the washcoat shown in Fig. 5 is considered as a single particle. Table 3 gives all other dimensions and properties of the monolith reactor used in the simulations.

7. Simulation results

In all cases external mass and heat transfer limitations were found to be negligible. Moreover, the calculations show that the washcoat layer is uniform in temperature. However, internal mass transfer limitations exist inside the washcoat depending on the operating conditions.

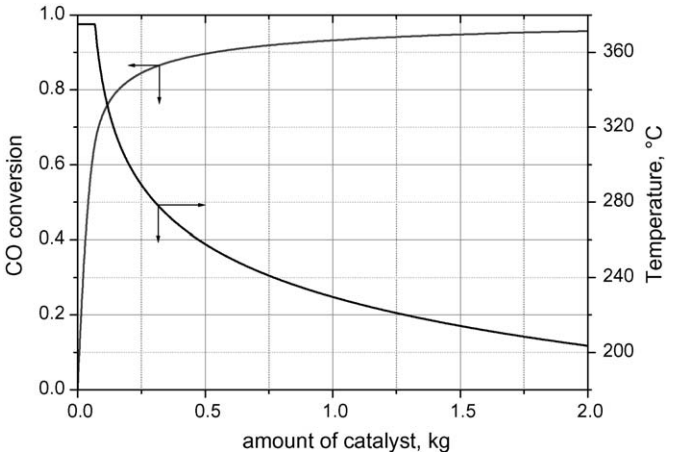

Fig. 6. Optimal temperature profile and the corresponding CO conversion as a function of the amount of catalyst.

If no additional water is injected, the optimal temperature path gives the smallest reactor size, single or multistage. Fig. 5 shows the axial temperature profile and the conversion versus catalyst amount for this reactor type with an inlet temperature of 375 °C. Approximately 0.5 kg of catalyst is necessary to reach 90% CO conversion (Fig. 6). This reactor is difficult to construct and operate but such a unit based on stainless steel microreactor technology has been reported [23].

Fig. 2 shows the three different adiabatic trajectories for the different reactor configurations considered. Curve A corresponds to a single stage for which an optimum inlet temperature of 172 °C has been calculated. Due to the low catalyst activity at these low initial temperatures 9.1 kg of washcoat is necessary to reach 90% conversion and the adiabatic temperature rise equals 110 °C.

Curve B corresponds to a dual stage reactor with intermediate cooling for which a maximum inlet temperature of 290 °C has been calculated. Higher inlet temperatures result in only a minor gain in reactor volume but the outlet temperature gets close to 400 °C thus leading to reduced catalyst lifetimes. The initial stage reaches an outlet temperature close to 375 °C and the optimum inlet temperature for the second stage is 260 °C. For the two stages combined 0.95 kg of catalyst is needed to reach 90% conversion. The position of the cooling is obtained by applying the Bellmans' principle that is stating that the reaction rate at the reactor outlet of stage 1 equals the reaction rate at the inlet of stage 2. In this case this corresponds to 0.23 kg of catalyst.

Curve C corresponds to dual stage with intermediate cooling by water injection. An optimum amount of water addition equal to 9 mmol s^{-1} has been calculated as shown in Fig. 7. Injecting more water will cool the reaction gas more than can be compensated by the gain in the shift of the thermodynamic equilibrium. The initial stage follows very closely curve B. The second stage has a higher inlet temperature and crosses the equilibrium curve in Fig. 2 due to the water addition. For the two stages combined 0.55 kg of catalyst is needed to reach 90% conversion. Fig. 3 summarizes the optimum inlet and outlet temperatures and catalyst amounts for the different reactor configurations.

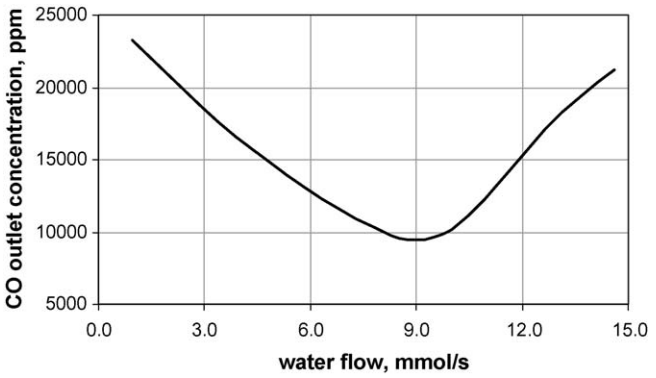

Fig. 7. The calculated CO outlet concentration as a function of the water addition to the second stage.

8. Fixed bed reactor

For onboard applications the catalyst needs to resist well against mechanical shocks and vibrations and therefore monoliths are the support of choice. However, it is interesting to compare the overall reactor size of a monolith-supported system to a fixed bed configuration to that. Due to its much higher porosity and the space taken by the cordierite itself the monolith-supported catalyst will generally result in larger reactor volumes. This can be compensated by the higher efficiency factors that can be obtained in the thin washcoat layers.

The optimum design of a packed bed reactor is often a trade-off between the pressure drop and the catalyst activity. Large particle sizes and large void fractions of the bed favor low pressure drops, but large particle sizes can lead to lower catalyst activity if internal concentration gradients are significant. Many different catalyst shapes are found for industrial use. A commonly used shape that presents a good compromise is the hollow cylinder. It is especially suited under conditions of diffusion control and large void fractions of the bed can be achieved [24]. The catalyst mass needed to achieve 90% CO conversion in a fixed bed reactor using hollow cylinders of different sizes has been calculated for a two-stage reactor with water addition. The ratio of the diameter to the length of the cylinder is set to 1 and the

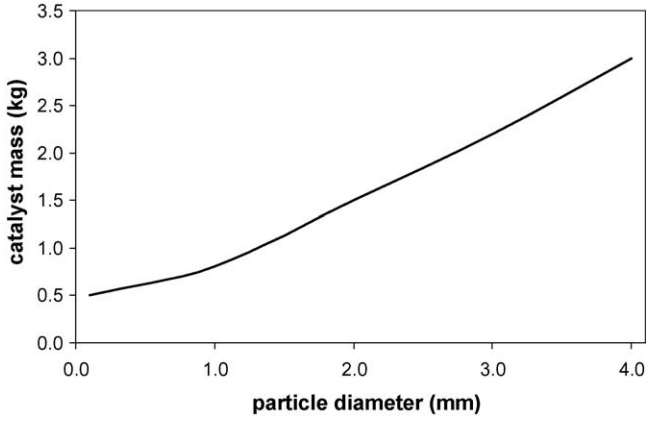

Fig. 8. Catalyst mass calculated to obtain 90% CO conversion in a fixed bed reactor using spherical catalyst particles.

ratio of the inner to outer diameter is fixed at 0.5. The catalyst efficiency is based on the equivalent particle diameter. Fig. 8 shows that the amount of catalyst necessary to obtain 90% CO conversion increases more than linearly with the equivalent particle diameter due to the increased internal diffusion limitations. Using 1.5 mm size particles leads to a fixed bed reactor that is larger in volume than a monolith-based system, whereas at 2.5 mm size particles a gain in weight can be expected by the use of monoliths. Industrial catalysts, however, will greatly benefit from a shell design where the platinum is deposited in a thin outer layer of the catalyst.

9. Conclusions

$Pt/CeO_2/Al_2O_3$ catalysts are cited as promising catalysts for CO clean-up for onboard applications as they are highly active and non-pyrophoric. The kinetics was measured over a $Pt/CeO_2/Al_2O_3$ catalyst in the absence of mass and heat transfer limitations. The experimental data could be described adequately in the form of a power rate law. This rate equation has been used to optimize an adiabatic monolith reactor. The reactor simulation takes into account the external and internal mass and heat transfer limitations. The experimentally obtained washcoat geometry has been modeled by a two equivalent particle approach to better describe the diffusion in the corner and side sections of the washcoat. Although Pt/ceria catalysts are quite active for the water–gas shift reaction their activity drops significantly below 250 °C which makes a single stage adiabatic reactor design exceptionally large. A two-stage adiabatic reactor design with additional water injection leads to a catalyst quantity similar to that of a reactor operating according to the optimal temperature path. A monolith-based design not only gives the required mechanical strength but also leads to better Pt utilization and thus smaller reactor volumes compared to a fixed bed configuration using industrial size catalysts.

References

[1] F.A. De Bruijn, Green Chem. 7 (3) (2005) 132–150.
[2] P. Trambouze, J.P. Euzen, Les réacteurs chimiques, de la conception à la mise en oeuvre, Edition Technip, 2002.
[3] A.F. Ghenciu, Curr. Opin. Solid State Mater. Sci. 6 (5) (2002) 389–399.
[4] Q. Fu, H. Saltsburg, M. Flytzani-Stephanopoulos, Science 301 (2003) 935–938.
[5] S. Hilaire, X. Wang, T. Luo, R.J. Gorte, J. Wagner, Appl. Catal. A 258 (2004) 271–276.
[6] A. Goguet, F.C. Meunier, D. Tibiletti, J.P. Breen, R. Burch, J. Phys. Chem. B 108 (2004) 20240–20246.
[7] G. Germani, P. Alphonse, M. Courty, Y. Schuurman, C. Mirodatos, Catal. Today 110 (1–2) (2005) 114–120.
[8] G.F. Froment, K.B. Bischoff, Chemical Reactor Analysis Design, second ed., Wiley, 1990.
[9] R.E. Hayes, S.T. Kolaczkowski, Introduction to Catalytic Combustion, Gordon and Breach Science Publishers, 1997.
[10] G. Groppi, A. Belloni, E. Troncani, P. Forzatti, Chem. Eng. Sci. 50 (17) (1995) 2705–2715.
[11] N. Wakao, S. Kaguei, Heat and Mass Transfer in Packed Beds, Gordon and Breach Science Publishers, 1982.
[12] O. Levenspiel, Chemical Reaction Engineering, third ed., John Wiley & Sons, Inc., 1999.
[13] R. Aris, Proc. R. Soc. Lond. Ser. A 235 (1956) 67–77.
[14] R.C. Reid, J.M. Prausnitz, B.E. Poling, The Properties of Gases and Liquids, fourth ed., McGraw Hill International, 1998.
[15] A.C. Hindemarsh, ODEPACK, A Systematized Collection of ODE Solvers, Elsevier, 1983.
[16] W.E. Schiesser, The Numerical Method of Lines, Academic Press, 1991.
[17] G. Germani, Y. Schuurman, AIChE J. 52 (2006) 1806.
[18] J.M. Moe, Chem. Eng. Prog. 58 (3) (1962) 33–36.
[19] D. Schweich (Ed.), Génie de la réaction chimique, TEC & DOC, 2001.
[20] R. Bellman, Dynamic Programming, Princeton University Press, 1957.
[21] R. Aris, The Optimal Design of Chemical Reactors, Academic Press, 1960.
[22] D. Leung, R.E. Hayes, S.T. Kolaczkowski, Can. J. Chem. Eng. 74 (1996) 94–103.
[23] W. TeGrotenhuis, K. Brooks, R. Dagle, J. Davis, J. Holladay, M. Kapadia, D. King, L. Pederson, B. Roberts, V. Stenkamp, DOE Hydrogen Program, FY 2004 Progress Report, 2004.
[24] R.J. Wijngaarden, A. Kronberg, K.R. Westerterp, Industrial Catalysis, Wiley/VCH, 1998.